Antarctic ice sheet sensitivity to atmospheric CO$_2$ variations in the early to mid-Miocene

Richard Levy[a,1], David Harwood[b], Fabio Florindo[c], Francesca Sangiorgi[d], Robert Tripati[e,f], Hilmar von Eynatten[g], Edward Gasson[h], Gerhard Kuhn[i], Aradhna Tripati[e,f], Robert DeConto[h], Christopher Fielding[b], Brad Field[a], Nicholas Golledge[a,j], Robert McKay[j], Timothy Naish[a,j], Matthew Olney[k], David Pollard[l], Stefan Schouten[m], Franco Talarico[n], Sophie Warny[o], Veronica Willmott[i], Gary Acton[p], Kurt Panter[q], Timothy Paulsen[r], Marco Taviani[s], and SMS Science Team[2]

[a]Department of Paleontology, GNS Science, Lower Hutt, New Zealand, 5040; [b]Department of Earth & Atmospheric Sciences, University of Nebraska, Lincoln, NE 68588; [c]Istituto Nazionale di Geofisica e Vulcanologia, I-00143 Rome, Italy; [d]Marine Palynology and Paleoceanography, Laboratory of Palaeobotany and Palynology, Department of Earth Sciences, Utrecht University, 3584 CD, Utrecht, The Netherlands; [e]Institute of the Environment and Sustainability, University of California, Los Angeles, CA 90024; [f]Department of Atmospheric and Oceanic Sciences, University of California, Los Angeles, CA 90095; [g]Department of Sedimentology & Environmental Geology, Geoscience Center Göttingen, 37077 Göttingen, Germany; [h]Department of Geosciences, University of Massachusetts, Amherst, MA 01003; [i]Alfred Wegener Institute for Polar & Marine Research, 27568 Bremerhaven, Germany; [j]Antarctic Research Centre, Victoria University of Wellington, Wellington, New Zealand, 6012; [k]Hillsborough Community College, Tampa, FL 10414; [l]Earth & Environmental Systems Institute, Pennsylvania State University, University Park, PA 16802; [m]Marine Organic Biogeochemistry, Royal Netherlands Institute for Sea Research, 1797 SZ 't Horntje (Texel), The Netherlands; [n]Dipartimento di Scienze Fisiche della Terra e dell'Ambiente, Università degli Studi di Siena, I-53100 Siena, Italy; [o]Department of Geology & Geophysics and Museum of Natural Science, Louisiana State University, Baton Rouge, LA 70803; [p]Department of Geography & Geology, Sam Houston State University, Huntsville, TX 77341; [q]Department of Geology, Bowling Green State University, Bowling Green, OH 43403; [r]Department of Geology, University of Wisconsin-Oshkosh, Oshkosh, WI 54901; and [s]Institute of Marine Sciences, National Research Council, 40129 Bologna, Italy

Geological records from the Antarctic margin offer direct evidence of environmental variability at high southern latitudes and provide insight regarding ice sheet sensitivity to past climate change. The early to mid-Miocene (23–14 Mya) is a compelling interval to study as global temperatures and atmospheric CO$_2$ concentrations were similar to those projected for coming centuries. Importantly, this time interval includes the Miocene Climatic Optimum, a period of global warmth during which average surface temperatures were 3–4 °C higher than today. Miocene sediments in the ANDRILL-2A drill core from the Western Ross Sea, Antarctica, indicate that the Antarctic ice sheet (AIS) was highly variable through this key time interval. A multiproxy dataset derived from the core identifies four distinct environmental motifs based on changes in sedimentary facies, fossil assemblages, geochemistry, and paleotemperature. Four major disconformities in the drill core coincide with regional seismic discontinuities and reflect transient expansion of grounded ice across the Ross Sea. They correlate with major positive shifts in benthic oxygen isotope records and generally coincide with intervals when atmospheric CO$_2$ concentrations were at or below preindustrial levels (~280 ppm). Five intervals reflect ice sheet minima and air temperatures warm enough for substantial ice mass loss during episodes of high (~500 ppm) atmospheric CO$_2$. These new drill core data and associated ice sheet modeling experiments indicate that polar climate and the AIS were highly sensitive to relatively small changes in atmospheric CO$_2$ during the early to mid-Miocene.

Antarctica | ice sheet | Climate Optimum | Ross Sea | Miocene

Knowledge regarding Antarctic ice sheet (AIS) response to warming climate is of fundamental importance due to the role ice sheets play in global sea level change. Paleoenvironmental records from Earth's past offer a means to examine AIS variability under climatic conditions that were similar to today and those projected for the next several decades (1, 2). In this respect, the early to mid-Miocene is a compelling interval to study as proxy reconstructions of atmospheric CO$_2$, albeit uncertain, suggest that concentrations generally varied between preindustrial levels (PAL = 280 ppm) and values at or above 500 ppm (3–9). Additionally, global mean surface temperature during peak Miocene warmth was up to 3–4° higher than today (10), similar to best-estimate temperatures expected by 2100 under the highest projected greenhouse gas concentration pathway (Representative Concentration Pathway 8.5) (1, 2). Finally, Miocene geography was similar to today (11), and major circum-Antarctic oceanic and

atmospheric circulation patterns that dominate the modern Southern Ocean were well established (12, 13).

Much of our understanding regarding AIS history through the early to mid-Miocene comes from far-field records from deep ocean basins. Benthic oxygen and carbon isotope proxies for global paleoclimate suggest that early to mid-Miocene climate and glacial environments were highly variable (14–19). These records include evidence for major transient glacial episodes and sea level fall, intervals of relative ice sheet stability, and periods of climatic warmth with major ice sheet retreat and sea level rise. Furthermore, reconstructions from sedimentary sequences on the Marion Plateau, offshore northeast Australia (20), and New Jersey margin (21) suggest sea level varied by up to 100 m. Episodes of sea level maxima (+40 m) suggest loss of Antarctica's marine-based ice sheets that, at present, occupy much of West Antarctica and large portions of East Antarctica (22), as well as

Significance

New information from the ANDRILL-2A drill core and a complementary ice sheet modeling study show that polar climate and Antarctic ice sheet (AIS) margins were highly dynamic during the early to mid-Miocene. Changes in extent of the AIS inferred by these studies suggest that high southern latitudes were sensitive to relatively small changes in atmospheric CO$_2$ (between 280 and 500 ppm). Importantly, reconstructions through intervals of peak warmth indicate that the AIS retreated beyond its terrestrial margin under atmospheric CO$_2$ conditions that were similar to those projected for the coming centuries.

substantial loss of mass from Antarctica's terrestrial ice sheets. Episodes of maximum sea level fall (up to −60 m) suggest that the AIS occasionally grew and advanced across continental shelves.

Geological records proximal to Antarctica's coastal margin provide direct evidence of past ice sheet variability in response to changing global climate. The ANDRILL (AND)-2A drill core, a 1,138-m-long stratigraphic archive of climate and ice sheet variability from the McMurdo Sound sector of the western Ross Sea (77°45.488′S, 165°16.613′E), was recovered by drilling from an ~8.5-m-thick floating sea ice platform in 380 m of water, located ~30 km off the coast of Southern Victoria Land (SVL) (Fig. 1A) (23). The drill core comprises lower Miocene to Quaternary glacial-marine strata deposited in the steadily subsiding Victoria Land Basin (VLB) (24). Paleogeography was broadly similar to today, although continental shelves in the Ross and Weddell seas were likely shallower (*SI Text* and Fig. S1). Recovered core sediments, and the proxies they contain, allow us to assess past ice sheet dynamics along a coastal margin influenced by ice flowing from East Antarctica and across the West Antarctic continental shelf. Through analysis of an integrated proxy environmental dataset, we derive a new environmental reconstruction and combine this with a suite of global environmental data to establish a history of AIS response to global climate events and episodes during the early to mid-Miocene. This integrated dataset allows us to evaluate key drivers of high latitude climate and ice sheet variability between 21 and 13 Ma. Outcomes from research reported here and in a companion ice sheet modeling study (25) suggest the AIS advanced across continental shelves during cold orbital configurations and retreated well inland of the coast under warm orbits. This large range of AIS variability occurred under a relatively low range in atmospheric CO_2 concentration (~280–500 ppm) and indicates the Antarctic environment was highly sensitive during the early to mid-Miocene.

Results

A near-continuous record spanning 20.2 to ~14.4 Ma is preserved in the lower 925 m of AND-2A (Fig. 1B, Figs. S2 and S3, and Table S1). A diverse range of geological information including physical properties and sedimentological, paleontological, and geochemical data were collected (summarized in *SI Text*, Table S2, and refs. 23 and 26–33). Here we present new data including sea surface water (upper 200 m) temperatures (SWTs) derived from archaeal lipids (TEX^L_{86}) (Fig. S4 and Table S3) and carbonate isotopes (Δ_{47}) (Table S4), whole rock inorganic geochemical data, and an integrated age model (Fig. S2 and Table S2), and offer the first analysis, to our knowledge, of a combined proxy environmental dataset derived from AND-2A (Fig. 1B and Fig. S3). These paleoenvironmental data are used to define four characteristic environmental motifs (EMs) (Table S2) that reflect distinct climatic and glacial regimes (Fig. 1 A and B).

Intervals of maximum ice sheet extent and cold polar conditions are assigned to EM I (maximum ice) and are characterized in AND-2A by four major disconformities. These disconformities are relatively rare and represent distinct and discrete times of major ice sheet advance beyond the drill site onto the continental shelf (Fig. 1 C, i). Three disconformities AND2A-U1 [965.43 m below sea floor (mbsf)]; -U2 (774.94 mbsf); and -U3 (262.57 mbsf) span the time intervals ~20–19.8, ~18.7–17.8, and ~15.8–14.6 Ma, respectively (Fig. S2). A fourth major disconformity AND2A-U4 (214.13 mbsf) separates middle Miocene rocks (>~14.4 Ma; Fig. S2) from 214 m of overlying upper Miocene to Quaternary strata.

Eight stratigraphic intervals in AND-2A are assigned to EM II (cold polar), as characterized by high magnetic susceptibility (MS), high Niobium (Nb) content, and low chemical index of alteration (CIA), all of which reflect sediment derived from local volcanic centers and unweathered outcrop in proximal regions of the Transantarctic Mountains (TAM). We infer that relative increases in local sediment are due to advance of ice from expanding ice caps on nearby Mount Morning and the Royal Society Range

under a cold polar climate. Five of the eight intervals are dominated by massive to stratified diamictite facies that often contain debris derived from local volcanic sources and were probably deposited beneath a floating ice tongue or ice shelf proximal to the grounding line of outlet or piedmont glaciers (Fig. 1 C, ii). Each of these intervals is typically fossil poor. TEX^L_{86}-derived SWTs range between −1.4 and 2.6 ± 2.8 °C and are supported by a Δ_{47}-derived value of 2.1 ± 3.7 °C at 366 mbsf. We infer that proxies in EM II reflect cold polar conditions with minimum grounding-line variability and persistent floating ice shelves and/or coastal fast ice.

Twelve stratigraphic intervals are assigned to EM III (cold temperate) as characterized by low to moderate MS, low to moderate Nb content, and moderate to high CIA. These data indicate variable sediment provenance and periodic input from local volcanic sources and/or unweathered outcrop. EM III is divided into subtypes a and b based on variations in lithofacies and fossil content. EM IIIa is dominated by stratified diamictite and gravel with variable clast composition but including a high proportion of rock fragments sourced from the region south of Skelton and Mulock glaciers. Foraminifera vary in abundance and are absent in many intervals but include up to 10 species in others (30). Marine diatoms and terrestrial palynomorphs are usually absent but occur in low abundance in several discrete intervals. Mollusc-bearing intervals are uncommon. TEX^L_{86}-derived SWTs range between 2.2 and 5.4 ± 2.8 °C. Intervals characterized by EM IIIa likely reflect a subpolar climate and glacial regime with tidewater glaciers. Periodic increase in gravel clasts derived from regions south of Mount Morning reflect an increase in ice flux through major East Antarctic ice sheet (EAIS) outlet valleys into fjords under warmer conditions. During these intervals, calving rates at the grounding-line increased and debris-laden icebergs delivered sediment to the drill site as they drifted northwards along the SVL coast (Fig. 1 C, iii).

EM IIIb has persistently low Nb and MS, reflecting minimal input from local volcanic sources. Lithofacies are diverse and include massive and stratified diamictite and gravel; clast composition is mixed, with a high proportion of lithologies derived from the Skelton and Mulock glaciers and as far south as the Carlyon and Byrd glaciers. Intervals of mudrock dominated sequences are more common in EM IIIb than in EM IIIa. Terrestrial palynomorphs are more abundant in several intervals of EMIIIb (e.g., 947.54, 922.61, and 593.29 mbsf), and discrete intervals bearing mollusc fossils occur occasionally (Fig. 1B and Fig. S3). TEX^L_{86}-derived SWTs range from 0.2 to 6.7 ± 2.8 °C. We infer that EM IIIb reflects a depositional setting similar to EM IIIa but with a generally warmer climate, particularly during periods when SWTs were 6–7 ± 2.8 °C and local ice cap margins retreated to the coast and had limited influence on marine sedimentation at the drill site. Coarse clastic sediment was primarily delivered to the drill site by debris-rich icebergs derived from large fast flowing outlet glaciers to the south. Increased abundance of *Podocarpites* spp. and *Nothofagidites* spp. pollen (Fig. 1B and Fig. S3) indicates local tundra occupied ice-free regions along the coastal margin (Fig. 1 C, iv).

Five relatively short, lithologically diverse, stratigraphic intervals are assigned to EM IV (minimum ice) as characterized by low MS, low Nb content, and high CIA, which indicate minimal sediment input from local volcanic sources and/or unweathered outcrop. Lithofacies are variable, but sequences are usually dominated by mudrock, sandstone, and thin diamictite. A 46-m-thick section between 996.69 and 1,042.55 mbsf incorporates five sequences dominated by sediments deposited within a marine-deltaic setting distal to the glacial margin (27). The interval between 428.28 and 436.18 mbsf incorporates a single sequence comprising a basal diamictite overlain by a sandstone unit with relatively abundant marine bivalves. Thick-shelled costate scallops and venerid clams recovered from this interval indicate that water temperatures were at least 5 °C warmer than in the
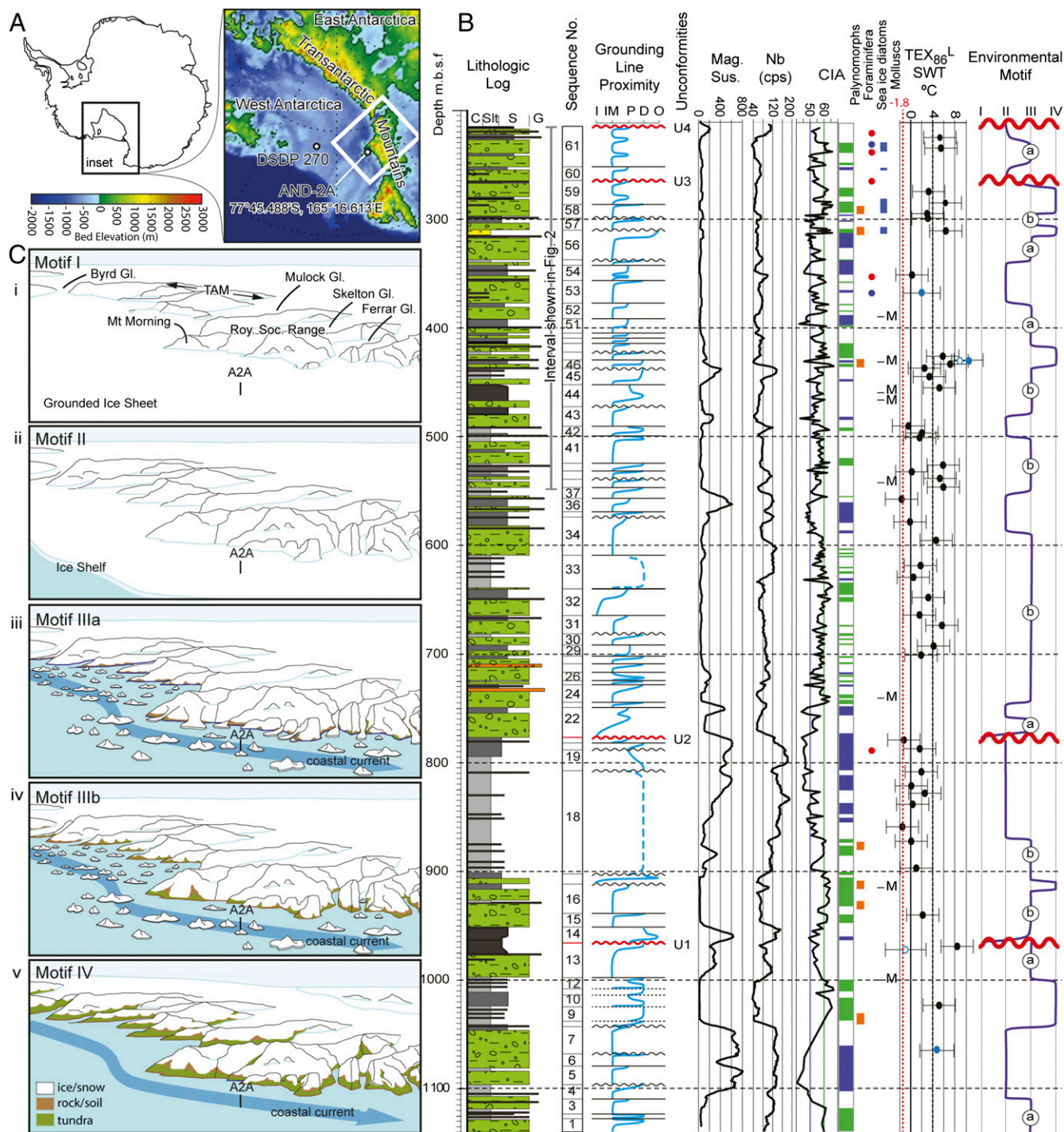
Fig. 1. (*A*) Map showing Ross Sea area (*Inset*) and AND-2A drill site (white box indicates approximate area for schematic reconstructions shown below). (*B*) Stratigraphic summary of lower 925 m of AND-2A (214.13–1,138.54 mbsf) showing 61 sedimentary cycles. Glacial proximity curve tracks relative position of the grounding line through ice-contact (I), ice-marginal (IM), ice-proximal (P), ice-distal (D), and open marine (O) environments. Continuously acquired datasets include magnetic susceptibility and Niobium (Nb) XRF-CS counts. CIA (curve and bar) indicates arid (<50, blue) and less arid (>60, green) conditions. Intervals of peak palynomorph concentration shown by orange boxes. Foraminifera assemblages include cold water/ice marginal benthic species (red circles) and cool water planktonic species (blue circles). Blue bars, sea ice diatoms; M, intervals with well-preserved molluscs. Sea water temperature estimates based on TEX$_{86}^L$ (black circles) and Δ_{47} (blue circles, open, less well-preserved specimens). Environmental Motif curve based on the proxy environmental dataset. (*C*) Schematic reconstructions of region around AND-2A showing likely conditions for each environmental motif (I–IV).

Ross Sea today (29). Relatively warm water temperatures are supported by TEX$_{86}^L$ and Δ_{47} data, which indicate SWT at the coastal margin reached a maximum between 7.0 ± 2.8 °C and 10.4 ± 2.5 °C. In situ pollen and spores are abundant in this interval and indicate a coastal vegetation of mossy tundra with shrub podocarps and southern beech and suggest a cool terrestrial climate (10 °C January mean air temperature) (31–33). Evidence for another interval of warm climate is also preserved in a unique diatom-rich unit at ~310 mbsf. This unit contains a typical tundra pollen assemblage recovered from other EM IV units but also

includes freshwater algae and cosmopolitan dinoflagellate taxa that indicate much warmer temperatures than occur in the Ross Sea today (32). Furthermore, TEX_{86}^L analyses from the diatomite unit indicate maximum surface water temperatures of ~6–7 ± 2.8 °C, which is consistent with values inferred from the fossils (29, 32) (*SI Text*). EM IV records times when the AIS margin retreated well inland and tundra occupied ice-free regions from the coast to at least 80 km inland (34)(Fig. 1 *C*, *v*).

Discussion

Proxy environmental data derived from AND-2A indicate coastal environments in SVL were highly variable throughout the early to mid-Miocene (Fig. 1 *B* and *C*). A robust age model for the AND-2A core (*Methods and Materials* and *SI Text*) allows us to integrate environmental data from the Antarctic coastal margin with regional seismic data from the Ross Sea continental shelf (35), deep sea oxygen and carbon isotope data (14, 15), sea level records (20), and atmospheric CO_2 reconstructions (3–9) (Fig. 2 and Fig. S5). We acknowledge that the age model for each dataset has uncertainties and caution that both proxy CO_2 reconstructions and sea level records are presently limited in temporal resolution and subject to large uncertainties. Despite these limitations, our correlation framework (Fig. 2 and Fig. S5) highlights several distinct episodes of (*i*) cold climate and marine-based ice sheet advance, (*ii*) peak warmth and maximum ice sheet retreat, and (*iii*) cold climate with relatively stable terrestrial ice sheets, which are discussed in detail below.

Four episodes of maximum ice sheet advance in the Ross Sea (MISA-1 to MISA-4) are documented between 21 and 13 Ma (Fig. 2 and Fig. S5). MISA episodes are recorded by stratigraphic gaps in AND-2A that correlate approximately in time with one of the major Ross Sea Unconformities (RSUs) that formed during ice sheet advance across the continental shelf (35). Each MISA episode also correlates generally with an interval of global sea level fall, enrichment in deep-sea benthic $\delta^{18}O$, increase in benthic $\delta^{13}C$ values, and decrease in bottom water temperature (BWT) (Fig. 2 and Fig. S5). These patterns suggest episodes of maximum ice sheet advance were not restricted to the Ross Sea but represent continental scale expansion of the AIS. Importantly, our correlation model suggests that these MISA episodes coincided generally with eccentricity minima and intervals when atmospheric CO_2 concentrations were below 300 ppm (4, 5). MISA-3 (~14.6–14.7 Ma) best illustrates these associations (Fig. 2) and is characterized by an ~30-m drop in sea level (20), a 2–3 °C decrease in BWT in the Southern Ocean (17), a 0.75‰ enrichment in $\delta^{18}O$, a major increase in $\delta^{13}C$ (CM 5 from ref. 18) and a decrease in atmospheric CO_2 concentration to ~300 ppm (4, 5). MISA-4 (~13.7–14.1 Ma) (Fig. S5) coincides with the major Mi-3/E3 oxygen isotope excursion (16, 19), a drop in sea level of ~60 m (20), a 2–3 °C decrease in BWT (17), and a drop in CO_2 below 300 ppm (3, 5) (Fig. 2 and Fig. S5). MISA-3 and -4 correspond in time with RSU 4, a surface that displays erosional features with relief similar to bathymetric troughs that formed beneath ice streams during recent glaciations (36). RSU 4 likely formed during a phase of ice sheet advance and retreat that began ~14.6 Ma and culminated in the Miocene Climate Transition (MCT) and maximum ice sheet advance at 13.8 Ma. This phase of cold climate and persistent marine-based ice sheets ended at ~10 Ma when ice retreated to the terrestrial margins as revealed by upper Miocene mud-rich sediments in AND-1B (37).

Five episodes of peak warmth (PW-1 to PW-5), during which AIS grounding-lines retreated inland of the coastal margin, are also recorded. PW episodes are characterized by warm climate indicators in AND-2A (EM IV) that coincide generally
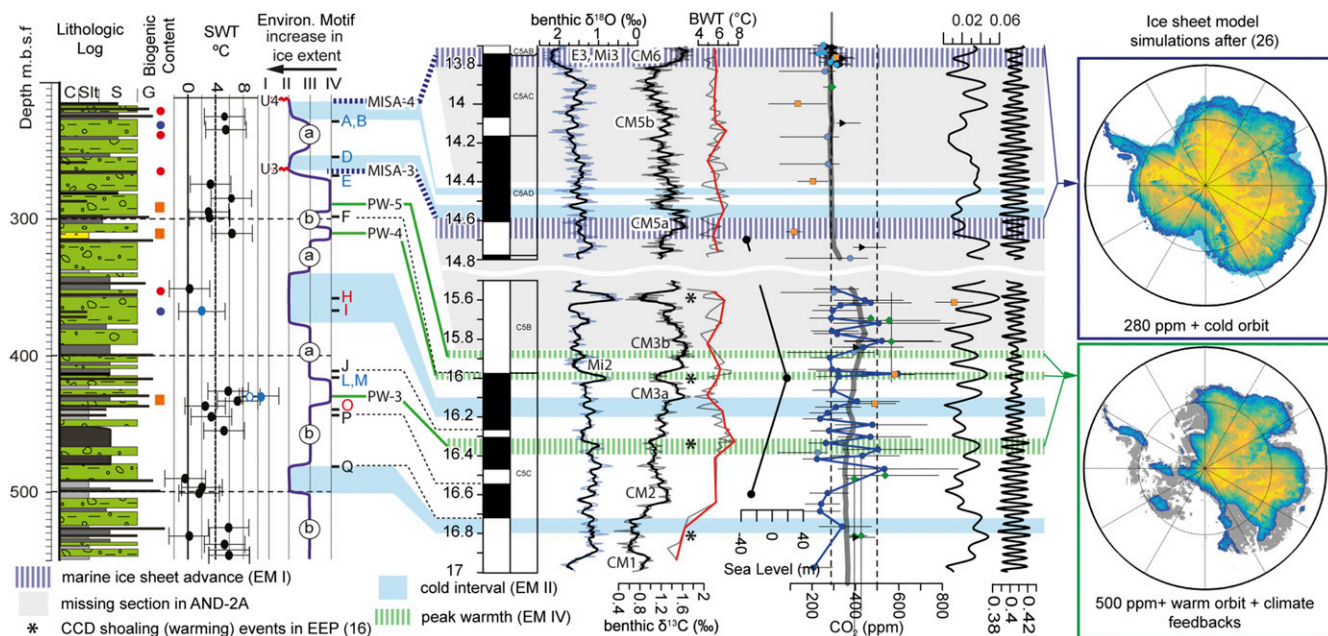

Fig. 2. Mid-Miocene section of AND-2A (557.35–214.13 mbsf) correlated to the Geomagnetic Polarity Timescale (46) and selected datasets. See Fig. 1 caption for description of AND-2A data. A–Q indicate position of key age model constraints (*SI Text*, Fig. S2, and Table S1). Benthic $\delta^{18}O$ and $\delta^{13}C$ isotope data with moving averages (thick lines) from IODP sites U1338 and U1337 (14, 15). Mi events after ref. 19 and E3 oxygen isotope excursion after ref. 16. CM, carbon isotope maxima (18, 39). Asterisks, carbon minima events and intervals of major shoaling of the carbonate compensation depth in the eastern equatorial Pacific (15). Bottom water temperature reconstructions from ref. 17 with 30-pt spline smooth (red line) (note: age model from ref. 17 adjusted by ~+50 ky for section between 15.5 and 17 Ma). Sea level data from the Marion Plateau (20). Proxy atmospheric CO_2 data include boron isotopes (3–5) (blue circles), alkenones (3, 6) (black triangles), stomata (7) (green diamonds), and paleosols (orange squares). Thick gray line = 21-point weighted average. Gray shaded boxes, time missing in unconformities; MISA (blue dashed line), maximum ice sheet advance (EMI); blue shaded zones, cold polar intervals (EMII); PW (green dashed line), peak warm intervals (EMIV). Orbital eccentricity and obliquity from ref. 48. Ice sheet simulations after ref. 25.

with times of elevated BWT, depleted $\delta^{18}O$ values, eccentricity maxima, low $\delta^{13}C$ values, and relatively high atmospheric CO_2 concentrations (Fig. 2 and Fig. S5). Intervals PW-3, -4, and -5 occurred between 16.4 and 15.8 Ma (Fig. 2) and offer insight into AIS response during the MCO. Ice-distal sediments in these intervals are relatively rich in terrestrial palynomorphs, and proxies indicate that SWTs in the Ross Sea were 6–10 °C warmer than today. PW-4 (16 Ma) best illustrates these relationships as it correlates with a major (∼0.5‰) decrease in $\delta^{18}O$, a 0.4‰ decrease in $\delta^{13}C$, a 2–3 °C increase in BWT at ODP site 1171 (17), and a 10- to 20-m rise in sea level across the Marion Plateau (20). Importantly, proxy data show that atmospheric CO_2 concentrations were >500 ppm during this warm episode (4, 7) (Fig. 2), which suggests that high latitude climate and Antarctica's terrestrial ice sheets were sensitive to CO_2 levels much lower than climate models suggest (38).

An unusual period of cold and relatively stable climate is suggested by proxies in the prominent thick interval of fine-grained sediments between 901.54 and 774.94 mbsf in AND-2A (sequence 18; Fig. 1B and Fig. S3). This unique stratigraphic interval is characterized by very low amounts of pollen and spores and persistently low SWTs (−1.3 °C to 2.6 °C). Foraminifera and diatoms are rare to absent. We infer the mudstone accumulated in a dark environment beneath semipermanent sea ice or an ice shelf. Interestingly, this interval correlates to upper Chron C6n, a time interval characterized by stable sea level (21) and low variability in orbital eccentricity (Fig. S5). Collectively, these data suggest that global climate and the AIS remained relatively stable through several glacial–interglacial cycles spanning at least 500 ky.

We conclude that environmental data from AND-2A and key far-field records indicate that Antarctica's climate and ice sheets were highly variable during the early to mid-Miocene. Whereas orbital variations were the primary driver of glacial cycles (28, 33, 39), atmospheric CO_2 variations modulated the extent of ice sheet advance and retreat. Specifically, coldest conditions and maximum ice sheet growth (MISA episodes and EM II) occurred generally during eccentricity minima and when atmospheric CO_2 was low (<400 ppm). Peak warmth and maximum AIS retreat occurred during eccentricity maxima and intervals of high CO_2 (≥500 ppm). Numerical climate and ice sheet model simulations produced in our companion study (25) (Fig. 2) support these observations and simulate grounding line advance across Antarctica's continental shelves under cold orbits and low CO_2 (280 ppm) but maximum retreat under warm orbital configuration and high CO_2 (500 ppm). Together, these studies suggest that polar climate and the AIS were highly sensitive to relatively small changes in atmospheric CO_2 during the early to mid-Miocene.

Summary

Our analysis of the AND-2A drill core and synthesis with regional and global data show that the early to mid-Miocene Antarctic coastal climate was highly variable. During relatively short-lived intervals of peak warmth, summer land surface air temperature was at least 10 °C, tundra vegetation extended to locations 80 km inland (34, 40), surface water temperatures in the Ross Sea were between 6 °C and 10 °C, and the AIS retreated inland. During intermittent intervals of peak cold climate, vegetation vanished and the AIS grew and advanced into the marine environment, expanding across the continental shelf.

Whereas glacial cycles were paced by orbital variability through the early to mid-Miocene, maximum ice sheet retreat occurred when atmospheric CO_2 was ≥500 ppm and maximum advance when CO_2 was ≤280 ppm (Fig. 2 and Fig. S5) (4). New numerical ice sheet simulations (25) also show that the Miocene AIS expanded across the continental shelf when atmospheric CO_2 was low (280 ppm) and retreated well inland of the coast when CO_2 was high (500 ppm). These ice sheet proximal data and model simulations support inferences from benthic deep sea records that suggest the global climate system and AIS were highly sensitive during the mid-Miocene (14–16). These results are consistent with observations and numerical climate and ice sheet simulations based on the warm Pliocene (41–44), which indicate that sustained levels of atmospheric CO_2 >400 ppm may represent a stability threshold for marine-based portions of the West and East Antarctic ice sheets. Furthermore, outcomes from our complementary drill core analysis and ice sheet modeling indicate that Antarctica's terrestrial ice sheets were vulnerable when atmospheric CO_2 concentrations last exceeded 500 ppm. Given current atmospheric CO_2 levels have risen above 400 ppm (45) and are projected to go higher (2), paleoclimate reconstructions such as this one for the early to mid-Miocene imply an element of inevitability to future polar warming, Antarctic ice sheet retreat, and sea level rise.

Methods and Materials

Methods are presented in detail in SI Text and ref. 23. AND-2A was described using standard sedimentological techniques to produce detailed stratigraphic logs (27). An age model for the core (Fig. S2) uses magnetostratigraphy, biostratigraphy, $^{87}Sr/^{86}Sr$ dating of macrofossils, and ^{40}Ar-^{39}Ar ages on lava clasts and tephra layers to correlate rock units to the Global Polarity Timescale (46). Assemblages of fossil pollen, dinoflagellates, diatoms, foraminifera, and molluscs were used to constrain paleoenvironmental conditions. A standard suite of continuous physical properties was collected on whole and split core and in the borehole. Whole rock inorganic geochemical data were collected at high sampling resolution using an X-ray fluorescence core scanner (XRF-CS). Additional chemical data were collected from discrete bulk sediment samples at lower resolution to provide calibration points for near-continuous noninvasive sampling obtained via XRF-CS. Concentrations of Al_2O_3, Na_2O, CaO, K_2O, P_2O_5, and total organic carbon (TOC) from bulk sediment samples were used to calculate the CIA (47). Samples for TEX^L_{86} were prepared at Utrecht University and LC-MS analyses performed at the Royal Netherlands Institute for Sea Research. Samples for Δ_{47} (clumped isotopes) were prepared and analyzed at the California Institute of Technology.

1. IPCC (2013) *Climate Change 2013: The Physical Science Basis. Contribution of Working Group 1 to the Fifth Assessment Report Intergovernmental Panel on Climate Change* (Cambridge Univ Press, Cambridge, UK).
2. Meinshausen M, et al. (2011) The RCP greenhouse gas concentrations and their extensions from 1765 to 2300. *Clim Change* 109(1-2):213–241.
3. Badger MPS, et al. (2013) CO2 drawdown following the middle Miocene expansion of the Antarctic Ice Sheet. *Paleoceanography* 28(1):42–53.
4. Greenop R, Foster GL, Wilson PA, Lear CH (2014) Middle Miocene climate instability associated with high-amplitude CO2 variability. *Paleoceanography* 29(9):2014PA002653.
5. Foster GL, Lear CH, Rae JWB (2012) The evolution of pCO2, ice volume and climate during the middle Miocene. *Earth Planet Sci Lett* 341–344(0):243–254.
6. Zhang YG, Pagani M, Liu Z, Bohaty SM, DeConto R (2013) A 40-million-year history of atmospheric CO2. *Philo Trans R Soc A: Math Phys Engineer Sci* 371(2001):1–20.

7. Kürschner WM, Kvaček Z, Dilcher DL (2008) The impact of Miocene atmospheric carbon dioxide fluctuations on climate and the evolution of terrestrial ecosystems. *Proc Natl Acad Sci USA* 105(2):449–453.
8. Retallack GJ (2009) Greenhouse crises of the past 300 million years. *Geol Soc Am Bull* 121(9-10):1441–1455.
9. Ekart DD, Cerling TE, Montanez IP, Tabor NJ (1999) A 400 million year carbon isotope record of pedogenic carbonate: Implications for paleoatmospheric carbon dioxide. *Am J Sci* 299(10):805–827.
10. You Y, Huber M, Müller RD, Poulsen CJ, Ribbe J (2009) Simulation of the Middle Miocene Climate Optimum. *Geophys Res Lett* 36(4):1–5.
11. Herold N, Seton M, Müller RD, You Y, Huber M (2008) Middle Miocene tectonic boundary conditions for use in climate models. *Geochem Geophys Geosyst* 9(10): Q10009.

12. Herold N, Huber M, Müller RD (2011) Modeling the Miocene Climatic Optimum. Part I: Land and atmosphere*. *J Clim* 24(24):6353–6372.

13. Herold N, Huber M, Müller RD, Seton M (2012) Modeling the Miocene climatic optimum: Ocean circulation. *Paleoceanography* 27(1):PA1209.

14. Holbourn A, et al. (2014) Middle Miocene climate cooling linked to intensification of eastern equatorial Pacific upwelling. *Geology* 42(1):19–22.

15. Holbourn A, Kuhnt W, Kochhann KGD, Andersen N, Sebastian Meier KJ (2015) Global perturbation of the carbon cycle at the onset of the Miocene Climatic Optimum. *Geology* 43(2):123–126.

16. Flower BP, Kennett JP (1993) Middle Miocene ocean-climate transition; high-resolution oxygen and carbon isotopic records from Deep Sea Drilling Project Site 588A, Southwest Pacific. *Paleoceanography* 8(6):811–843.

17. Shevenell AE, Kennett JP, Lea DW (2008) Middle Miocene ice sheet dynamics, deep-sea temperatures, and carbon cycling: A Southern Ocean perspective. *Geochem Geophys Geosyst* 9(2):Q02006.

18. Woodruff F, Savin S (1991) Mid-Miocene isotope stratigraphy in the deep sea: High-resolution correlations, paleoclimatic cycles, and sediment preservation. *Paleoceanography* 6(6):755–806.

19. Miller KG, Wright JD, Faribanks RG (1991) Unlocking the ice house: Oligocene-Miocene oxygen isotopes, eustasy, and margin erosion. *J Geophys Res* 96(B4):6829–6848.

20. John CM, et al. (2011) Timing and magnitude of Miocene eustasy derived from the mixed siliciclastic-carbonate stratigraphic record of the northeastern Australian margin. *Earth Planet Sci Lett* 304(3–4):455–467.

21. Kominz MA, et al. (2008) Late Cretaceous to Miocene sea-level estimates from the New Jersey and Delaware coastal plaoin coreholes: An error analysis. *Basin Res* 20: 211–226.

22. Fretwell P, et al. (2013) Bedmap2: Improved ice bed, surface and thickness datasets for Antarctica. *The Cryosphere* 7(1):375–393.

23. Harwood D, Florindo F, Talarico F, Levy RH, eds (2008–2009) Studies from the ANDRILL Southern McMurdo Sound Project, Antarctica. Initial Science Report on AND-2A. *Terra Antartica* 15(1):235.

24. Fielding CR, Whittaker J, Henrys SA, Wilson TJ, Naish TR (2008) Seismic facies and stratigraphy of the Cenozoic succession in McMurdo Sound, Antarctica: Implications for tectonic, climatic and glacial history. *Palaeogeogr Palaeoclimatol Palaeoecol* 260(1):8–29.

25. Gasson E, DeConto RM, Pollard D, Levy RH (2016) Dynamic Antarctic ice sheet during the early to mid-Miocene. *Proc Natl Acad Sci USA* 113:3459–3464.

26. Passchier S, et al. (2011) Early and middle Miocene Antarctic glacial history from the sedimentary facies distribution in the AND-2A drill hole, Ross Sea, Antarctica. *Geol Soc Am Bull* 123(11-12):2352–2365.

27. Fielding CR, et al. (2011) Sequence stratigraphy of the ANDRILL AND-2A drillcore, Antarctica: A long-term, ice-proximal record of Early to Mid-Miocene, sea-level and glacial dynamism. *Palaeogeogr Palaeoclimatol Palaeoecol* 305(1-4):337–351.

28. Passchier S, Falk CJ, Florindo F (2013) Orbitally paced shifts in the particle size of Antarctic continental shelf sediments in response to ice dynamics during the Miocene climatic optimum. *Geosphere* 9(1):54–62.

29. Beu A, Taviani M (2013) Early Miocene Mollusca from McMurdo Sound, Antarctica (ANDRILL 2A drill core), with a review of Antarctic Oligocene and Neogene Pectinidae (Bivalvia). *Palaeontology* 57(2):299–342.

30. Patterson MO, Ishman SE (2012) Neogene benthic foraminiferal assemblages and paleoenvironmental record for McMurdo Sound, Antarctica. *Geosphere* 8(6): 1331–1341.

31. Feakins SJ, Warny S, Lee J-E (2012) Hydrologic cycling over Antarctica during the middle Miocene warming. *Nat Geosci* 5(8):557–560.

32. Warny S, et al. (2009) Palynomorphs from a sediment core reveal a sudden remarkably warm Antarctica during the middle Miocene. *Geology* 37(10):955–958.

33. Griener KW, Warny S, Askin R, Acton G (2015) Early to middle Miocene vegetation history of Antarctica supports eccentricity-paced warming intervals during the Antarctic icehouse phase. *Global Planet Change* 127(0):67–78.

34. Lewis AR, Ashworth AC (2015) An early to middle Miocene record of ice-sheet and landscape evolution from the Friis Hills, Antarctica. *Geol Soc Am Bull*, 10.1130/B31319.1.

35. De Santis L, Anderson JB, Brancolini G, Zayatz I (1995) *Seismic Record of Late Oligocene Through Miocene Glaciation on the Central and Eastern Continental Shelf of the Ross Sea. Geology and Seismic Stratigraphy of the Antarctic Margin* (AGU, Washington, DC), Vol 68, pp 235–260.

36. Anderson JB, Bartek LR (1992) *Cenozoic Glacial History of the Ross Sea Revealed by Intermediate Resolution Seismic Reflection Data Combined with Drill Site Information. The Antarctic Paleoenvironment: A Perspective on Global Change*, eds Kennett JP, Warnke DA (American Geophysical Union, Washington, DC), Vol 56, pp 231–263.

37. McKay R, et al. (2009) The stratigraphic signature of the late Cenozoic Antarctic Ice Sheets in the Ross Embayment. *Geol Soc Am Bull* 121(11-12):1537–1561.

38. Goldner A, Herold N, Huber M (2014) The challenge of simulating the warmth of the mid-Miocene climatic optimum in CESM1. *Clim Past* 10(2):523–536.

39. Holbourn A, Kuhnt W, Schulz M, Erlenkeuser H (2005) Impacts of orbital forcing and atmospheric carbon dioxide on Miocene ice-sheet expansion. *Nature* 438(7067): 483–487.

40. Lewis AR, et al. (2008) Mid-Miocene cooling and the extinction of tundra in continental Antarctica. *Proc Natl Acad Sci USA* 105(31):10676–10680.

41. Naish T, et al. (2009) Obliquity-paced Pliocene West Antarctic ice sheet oscillations. *Nature* 458(7236):322–328.

42. Cook CP, et al. (2013) Dynamic behaviour of the East Antarctic ice sheet during Pliocene warmth. *Nat Geosci* 6(9):765–769.

43. Pollard D, DeConto RM (2009) Modelling West Antarctic ice sheet growth and collapse through the past five million years. *Nature* 458(7236):329–332.

44. Pollard D, DeConto RM, Alley RB (2015) Potential Antarctic Ice Sheet retreat driven by hydrofracturing and ice cliff failure. *Earth Planet Sci Lett* 412(0):112–121.

45. Dlugokencky E, Tans P (2016) Trends in Atmospheric Carbon Dioxide. Available at www.esrl.noaa.gov/gmd/ccgg/trends/.

46. Ogg JG (2012) Geomagnetic polarity time scale. *The Geologic Time Scale*, eds Gradstein FM, Schmitz JGOD, Ogg GM (Elsevier, Boston), pp 85–113.

47. Nesbitt HW, Young GM (1982) Early Proterozoic climates and plate motions inferred from major element chemistry of lutites. *Nature* 299(5885):715–717.

48. Laskar J, Fienga A, Gastineau M, Manche H (2011) La2010: A new orbital solution for the long-term motion of the Earth. *Astron Astrophys* 532(A89):1–15.

49. Wilson DS, et al. (2012) Antarctic topography at the Eocene-Oligocene boundary. *Palaeogeogr Palaeoclimatol Palaeoecol* 335-336(2012):24–34.

50. Sugden D, Denton G (2004) Cenozoic landscape evolution of the Convoy Range to Mackay Glacier area, Transantarctic Mountains: Onshore to offshore synthesis. *Geol Soc Am Bull* 116(7-8):840–857.

51. Levy RH, et al. (2012) Late Neogene climate and glacial history of the Southern Victoria Land coast from integrated drill core, seismic and outcrop data. *Global Planet Change* 80-81(Special Issue):61–84.

52. Fitzgerald PG (1992) The Transantarctic Mountains of southern Victoria Land: The application of apatite fission track analysis to a rift shoulder uplift. *Tectonics* 11(3): 634–662.

53. Kyle PR, Muncy HL (1989) Geology and geochronology of McMurdo Volcanic Group rocks in the vicinity of Lake Morning, McMurdo Sound, Antarctica. *Antarct Sci* 1(04): 345–350.

54. Marcano MC, et al. (2009) Chronostratigraphic and paleoenvironmental constraints derived from the 87Sr/86Sr signal of Miocene bivalves, Southern McMurdo Sound, Antarctica. *Global Planet Change* 69(3):124–132.

55. Di Vincenzo G, Bracciali L, Del Carlo P, Panter K, Rocchi S (2009) 40Ar-39Ar dating of volcanogenic products from the AND-2A core (ANDRILL Southern McMurdo Sound Project, Antarctica): Correlations with the Erebus Volcanic Province and implications for the age model of the core. *Bull Volcanol* 72:487–505.

56. Florindo F, et al. (2013) Paleomagnetism and biostratigraphy of sediments from Southern Ocean ODP Site 744 (southern Kerguelen Plateau): Implications for early-to-middle Miocene climate in Antarctica. *Global Planetary Change* 110(0):434–454.

57. Talarico FM, Sandroni S (2011) Early Miocene basement clasts in ANDRILL AND-2A core and their implications for paleoenvironmental changes in the McMurdo Sound region (western Ross Sea, Antarctica). *Global Planet Change* 78(1–2):23–35.

58. Hauptvogel DW, Passchier S (2012) Early–Middle Miocene (17–14 Ma) Antarctic ice dynamics reconstructed from the heavy mineral provenance in the AND-2A drill core, Ross Sea, Antarctica. *Global Planet Change* 82–83:38–50.

59. Roser BP, Pyne AR (1989) Wholerock geochemistry. *Antarctic Cenozoic History from the CIROS-1 Drillhole, McMurdo Sound, DSIR Bulletin*, ed Barrett PJ (DSIR Publishing, Wellington, New Zealand), Vol 245, pp 175–184.

60. Bahlburg H, Dobrzinski N (2011) A review of the Chemical Index of Alteration (CIA) and its application to the study of Neoproterozoic glacial deposits and climate transitions. *Geol Soc Lond Mem* 36(1):81–92.

61. Schouten S, Hopmans EC, Schefuß E, Sinninghe_Damste JS (2002) Distributional variations in marine crenarchaeotal membrane lipids: A new tool for reconstructing ancient sea water temperatures. *Earth Planet Sci Lett* 204:265–274.

62. Kim J-H, et al. (2010) New indices and calibrations derived from the distribution of crenarchaeal isoprenoid tetraether lipids: Implications for past sea surface temperature reconstructions. *Geochim Cosmochim Acta* 74(16):4639–4654.

63. Kim J-H, et al. (2012) Holocene subsurface temperature variability in the eastern Antarctic continental margin. *Geophys Res Lett* 39(6):L06705.

64. Kalanetra KM, Bano N, Hollibaugh JT (2009) Ammonia-oxidizing Archaea in the Arctic Ocean and Antarctic coastal waters. *Environ Microbiol* 11(9):2434–2445.

65. Tierney JE, Tingley MP (2014) A Bayesian, spatially-varying calibration model for the TEX86 proxy. *Geochim Cosmochim Acta* 127:83–106.

66. Hopmans EC, et al. (2004) A novel proxy for terrestrial organic matter in sediments based on branched and isoprenoid tetraether lipids. *Earth Planet Sci Lett* 224(1–2): 107–116.

67. Eagle RA, et al. (2013) The influence of temperature and seawater carbonate saturation state on 13C–18O bond ordering in bivalve mollusks. *Biogeosciences* 10(7): 4591–4606.

68. Kim ST, O'Neil JR (1997) Equilibrium and non-equilibrium oxygen isotope effects in synthetic carbonates. *Geochim Cosmochim Acta* 61:3461–3475.

69. Marcano MC, Frank TD, Mukasa SB, Lohmann KC, Taviani M (2015) Diagenetic incorporation of Sr into aragonitic bivalve shells: Implications for chronostratigraphic and palaeoenvironmental interpretations. *The Depositional Record* 1(1):38–52.

70. Frank TD, Gui Z, ANDRILL SMS Science Team (2010) Cryogenic origin for brine in the subsurface of southern McMurdo Sound, Antarctica. *Geology* 38(7):587–590.

71. Liebrand D, et al. (2011) Antarctic ice sheet and oceanographic response to eccentricity forcing during the early Miocene. *Clim Past* 7(3):869–880.